



## Two-DOF magnetic orientation sensor using distributed multipole models for spherical wheel motor

Hungsun Son <sup>a,\*</sup>, Kok-Meng Lee <sup>b</sup>

<sup>a</sup> School of Mechanical and Aerospace Engineering, Nanyang Technological University, Singapore

<sup>b</sup> Woodruff School of Mechanical Engineering, Georgia Institute of Technology, Atlanta, GA, USA

### ARTICLE INFO

#### Article history:

Received 30 April 2009

Accepted 5 October 2010

Available online 3 November 2010

#### Keywords:

Hall sensor

Magnetic field

Magnetic dipole

Orientation

Position

Spherical wheel motor

### ABSTRACT

This paper presents a new method for measuring a two degree-of-freedom (DOF) orientation of a permanent magnet (PM) based system using magnetic field measurements. The method exploits distributed multipole (DMP) modeling method to accurately predict a magnetic field, and provides a rational basis to inversely solve for the orientation of the PM from measured data. The PM-based magnetic sensor along with the ability to characterize the magnetic field in real-time offers advantages in sensing and control such as contact-free measurements eliminating frictional wears commonly encountered in existing designs with a combination of single-axis encoders, and high-speed sampling rate thus offering a higher bandwidth than methods based on imaging sensors. This paper demonstrates the efficient method capable of measuring the orientation of the PM by implementing it on a spherical wheel motor (SWM), where the two-DOF orientation is measured. Sensor performance has been studied both analytically and experimentally to validate the DMP-based sensor model. The results can offer valuable insights for optimizing contact-free sensor designs.

© 2010 Elsevier Ltd. All rights reserved.

### 1. Introduction

Many modern devices rely on a magnetic sensor to measure their orientation/position for accurate motion control since it offers a number of advantages including contactless, compact, robust and low cost. However, position/orientation measurements using the magnetic sensor have many difficulties in particular for multi-axis applications (such as machine tools, automation equipments, gyroscope, mobile vehicles and medical instruments) because they involve accurately estimating magnetic fields and solving the inverse model which seeks the solution from measured magnetic data analytically or numerically in real-time. To be effective, methods to solve the inverse model for magnetic sensors not only must be computationally efficient but also accurate; the problem remains a challenge to be solved.

Numerous techniques for orientation/position sensing have been widely developed using an excitation magnetic source such as a coil modeled as a dipole [1,2] where the principle of measurement is based on analyzing both phase lock loop and amplitude between originally excited and measured signals. In general, the phase-locking method provides good tracking accuracy but often requires additional devices including a power supply and electric wire connected to the coil. In addition, the magnetic field is relatively weak (mainly due to heat generation) as compared to that

of a permanent magnet (PM) for the same volume. An effective alternative is the use of a PM as the source to provide a strong magnetic field without any power source and electric wire, which enables the system to be more compactly designed. Traditionally, constant-field magnetic sensors have been dominant in a single-axis rotary machine [3,4] for position sensing but recently several studies involving three-dimensional position detection have been developed in diverse applications [5–9]. In [6], a linear algorithm has been proposed to trace the magnet position and orientation for medical applications. This research employs a number of three-axis magnetic sensors, and utilizes an optimized algorithm to detect the local magnetic field in real-time. In addition to the sensing method, a compact magnetic sensor has been developed in [7] to measure both a magnetic field and its spatial gradient tensor simultaneously, and to detect the orientation and position of the PM. As a practical application, a noncontact joystick with a PM and a hall sensor has been developed to measure its orientation in [10,11]. In most of these studies, a single dipole approximation (or an empirical formulation) is commonly used since it offers a simple closed-form solution to characterize the magnetic field for computing the position in three-dimensional space. While the single dipole has been widely used to analyze a magnetic field at a sufficiently large distance [12,13], it generally gives a poor approximation when the length-scale of the field is relatively small.

Recently, Lee and Son [14,15] developed a new modeling method (referred to here as distributed multipoles or DMP) to derive closed-form solutions for characterizing magnetic fields of a PM

\* Corresponding author. Tel.: +65 67905508; fax: +65 67924062.

E-mail address: [hsson@ntu.edu.sg](mailto:hsson@ntu.edu.sg) (H. Son).

## Nomenclature

### Capitalized symbols

<b>B</b>	magnetic flux density
$\hat{B}$	approximated magnetic flux density
<b>J</b>	Jacobian matrix
<b>P</b>	position vector of interest
$\mathbf{P}_{ji\pm}$	position vector of the $i$ th dipole in the $j$ th loop
$\mathbf{S}_{X\pm}/\mathbf{S}_{Y\pm}$	sensor position vector
$S_x$	$\sin(x)$
$C_x$	$\cos(x)$
$\mathbf{M}_o$	magnetization vector
<b>W</b>	weighting matrix
XYZ	inertial coordinate
$S$	distance of sensor location in XY plane
$Z_s$	Z coordinate of sensor location

### Lowercase symbols

$a$	radius of PM
-----	--------------

$l$	length of PM
$\mathbf{m}$	dipole strength
$m$	mass of the stage
$n$	number of dipole in the loops
$k$	number of dipole loops
$\mathbf{q}_R$	rotation vector
$k_c$	sensor conversion factor
$k_s$	number of sensors
xyz	moving coordinate with PM
$\mathbf{q}$	orientation vector

### Greek letter symbols

$\Gamma(\mathbf{q})$	coordinate transformation matrix
$\alpha, \beta, \gamma$	ZYZ Euler angles
$\mu_o$	free space permeability

using a set of dipoles for designing a PM-based device. The DMP method which inherits many advantages of the dipole model originally conceptualized in the context of physics provides an effective means to account for the shape and magnetization of the physical magnet. The DMP method has been validated against published (numerical, experimental and analytically known) solutions in [14] and additional applications illustrating the method can be found in [15].

In this paper, we exploit the DMP model to predict magnetic fields to develop a two-DOF orientation sensor originally proposed in [16]. Specifically, the sensor consisting of multiple Hall-effect elements is implemented at a PM-based multi-DOF actuator to measure its orientation. As will be shown, comparisons between theoretically calculated orientations against experimental measurements show good agreements.

## 2. Magnetic field for sensor formulation

Fig. 1a shows the PM-based orientation sensor consisting of a moving PM and a magnetic sensor located at  $\mathbf{P}$ . As an illustration, we consider here a cylindrical PM (of radius  $a$  and length  $l$ ) for the moving PM and model it using  $k$  circular loops (each with radius  $\bar{a}_j$  and  $n$  dipoles parallel to the magnetization vector  $M_o\mathbf{z}$ ) as shown in Fig. 1b. The  $k$  loops are uniformly spaced of  $\bar{a}_j = aj/(k+1)$  at  $z = \pm l/2$ , where  $j = 0, 1, \dots, k$ , and  $0 < l < l$ . Using the DMP modeling method [14], the closed-form solution characterizing the magnetic flux density  $\mathbf{B}$  of the cylindrical PM is given by equation:

$$\mathbf{B} = \frac{\mu_o}{4\pi} \sum_{j=0}^k m_j \sum_{i=1}^n \left( \frac{\mathbf{a}_{Rji+}}{R_{ji+}^2} - \frac{\mathbf{a}_{Rji-}}{R_{ji-}^2} \right) \quad \text{where} \quad \frac{\mathbf{a}_{Rji\pm}}{R_{ji\pm}^2} = -\frac{\mathbf{P} - \mathbf{P}_{ji\pm}}{|\mathbf{P} - \mathbf{P}_{ji\pm}|^3} \quad (1ab)$$

where  $\mu_o$  is the permeability of free space,  $m_j$  is the dipole moment in the  $j$ th loop;  $\mathbf{P} - \mathbf{P}_{ji\pm}$  is the position vector from the  $i$ th dipole in the  $j$ th loop to arbitrary position  $\mathbf{P}(x, y, z)$  of interest; and  $R_{ji\pm} = |\mathbf{P} - \mathbf{P}_{ji\pm}|$ .

In Fig. 1a,  $L$  is distance between center of the PM and origin of the XYZ coordinates. The PM rotates along with the xyz frame and its moving magnetic field in (1a,b) is expressed in the XYZ frame. Due to the symmetry of the magnetic field of the PM along the  $z$ -axis, only two orientation angles ( $\alpha$  and  $\beta$  in Fig. 1a) can be

measured. For the moving PM, the coordinate transformation from the xyz frame to the XYZ reference frame are described by (2):

$$\mathbf{P} = \Gamma(\mathbf{q})\mathbf{p} \quad (2)$$

where  $\Gamma(\mathbf{q}) = \begin{pmatrix} C_\beta & S_\alpha S_\beta & -C_\alpha S_\beta \\ 0 & C_\alpha & S_\alpha \\ S_\beta & -S_\alpha C_\beta & C_\alpha C_\beta \end{pmatrix}$ ;  $\mathbf{q} = [\alpha, \beta]$  is the orientation

vector in terms of xyz Euler angles,  $\mathbf{p}$  is the position of the PM expressed in the local xyz frame.  $C$  and  $S$  represent a cosine and a sine function respectively; and the subscripts of  $C$  and  $S$  denote their respective angles.

Eq. (1ab) with the position vector defined by (2) provide a means to determine the unknown orientation  $\mathbf{q}$  from magnetic flux density  $\mathbf{B}$  using a field-based sensor. However, the unknown orientation  $\mathbf{q}$  must be solved explicitly from the measurement of  $\mathbf{B}$ . In [15], an incremental method based on the gradient of magnetic fields has been proposed to track a PM. In this method, the orientation is measured without any approximation and change on Eq. (1ab). However, it requires a fast sampling rate and also has an intrinsic disadvantage of cumulative errors. An alternative to overcome these difficulties is to solve an inverse problem for absolute orientation in real-time by approximating the measured magnetic field density  $\mathbf{B}$  as a polynomial function  $\hat{B}$  with respects to the orientation angles  $\alpha$  and  $\beta$ .

Design concept is illustrated with an example in Fig. 2 which shows a two single-axis sensor-pairs placed symmetrically on the  $X$  and  $Y$  axes. The objective of the two-DOF orientation sensor is to measure the two orthogonal rotational displacements of the moving PM relative to magnetic sensors for a spherical wheel motor which requires sensing the orientation of the rotor. The magnetic field of the axially magnetized PM on the tip of the rotor is nonlinear in three-dimensional space but it travels with the moving PM that has circular motions due to the constant  $L$  (offset distance from the origin to the center of the PM). Evidently, the function  $\hat{B}$  represents the approximated magnetic field measured by the sensor, whose strength is inversely proportional to the distance from the PM and the sensor but in general it is not linear. Thus, if a pair of the sensors is placed symmetrically with respect to the PM, the magnetic field can be better approximated by an  $n$ th order polynomial in terms of sinusoid functions of  $\alpha$  and  $\beta$  compared to the rational polynomial function of the angles. The sensor-pairs with locations defined by Eq. (3ab) measure the magnetic field  $B_x$  and  $B_y$  respectively:

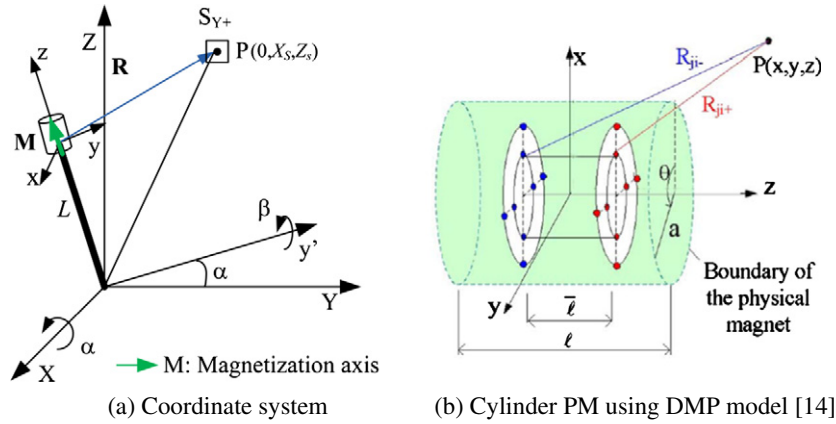


Fig. 1. Coordinate system illustrating the DMP model.

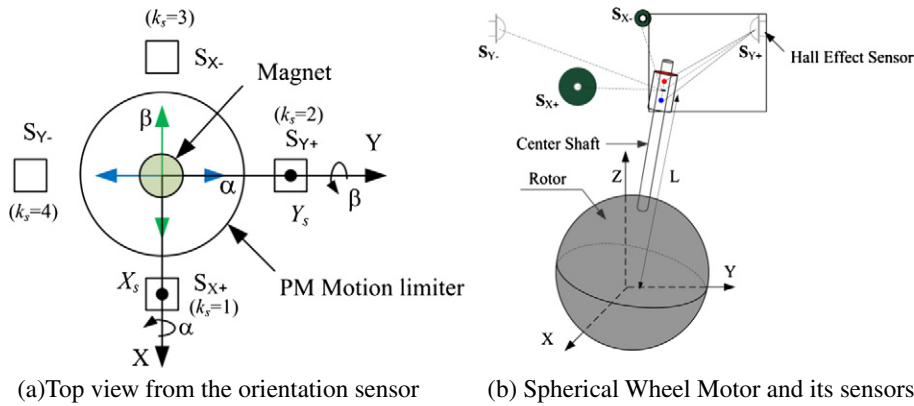


Fig. 2. Schematic design of orientation measurement for spherical wheel motor.

$$\mathbf{S}_{X\pm} = [\pm S \ 0 \ Z_s]^T \text{ and } \mathbf{S}_{Y\pm} = [0 \ \pm S \ Z_s]^T \quad (3ab)$$

where  $S$  is the distance of the sensor location in the  $XY$  plane and  $Z_s$  is the  $Z$  coordinate of the sensor locations defined in Fig. 1a, and the subscripts  $X\pm$  and  $Y\pm$  denote the sensor-pairs on the  $\pm X$  and  $\pm Y$  axes respectively. The locations of the sensors and the PM can be chosen to minimize the effect of other PMs (mainly rotor PMs) on the sensor measurement. The rotor PMs make an influence on sensor measurement, which reduces the accuracy when the length of  $L$  in Fig. 2 is short. In order to avoid the interaction of both the sensing PM and rotor PMs and thus obtain accurate measurement,  $L$  should be long enough to minimize the effect. On the other hand, if  $L$  is too long, it may cause an effect on dynamic responses as well as the stability of the rotor since the center of gravity is higher than the center of rotation. In addition, a measured signal becomes weaker. Thus, the moving PM and sensors should be optimally located.

### 2.1. Measured B-field approximation

For the sensor-pairs shown in Fig. 2,  $B_x$  (measured by the sensors at  $\mathbf{S}_{X\pm}$ ) can be expressed in an even function of  $\alpha$  due to the symmetric motion with respect to the sensors, but an odd function of  $\beta$  due to the asymmetric motion, and vice versa for  $B_y$  located at  $\mathbf{S}_{Y\pm}$ . Thus, the measured data due to the circular motion of the PM are approximated by following equations.

$$\hat{B}_X(\alpha, \beta) \Big|_{\mathbf{S}_{X\pm}} = \sum_{i=0}^n \sum_{j=0}^n c_{ij} (\cos \alpha)^i (\pm \sin \beta)^j \quad (4a)$$

$$\hat{B}_Y(\alpha, \beta) \Big|_{\mathbf{S}_{Y\pm}} = \sum_{i=0}^n \sum_{j=0}^n c_{ij} (\pm \sin \alpha)^j (\cos \beta)^i \quad (4b)$$

where  $n$  is the approximation order.

Using the least-square method, the coefficients  $c_{ij}$  in (4a) and (4b) can be obtained by minimizing the summed squared error:

$$E_k = \sum_{i=1}^n \sum_{j=1}^n [B_{k_s}(\alpha, \beta) - \hat{B}_{k_s}(\alpha, \beta)]^2 \quad (5)$$

where  $B_{k_s}(\alpha, \beta)$  is the analytical solution in (1ab),  $\hat{B}_{k_s}(\alpha, \beta)$  is from (4a) and (4b); and the subscript  $k_s$  denotes the  $k_s^{\text{th}}$  sensor (illustrated in Fig. 1a).

### 2.2. Approximate solution to the inverse problem

Once the approximated  $\hat{B}$  in (4a), (4b) and (5) is modeled, the orientation ( $\alpha$  and  $\beta$ ) can be obtained by solving the inverse problem; the solution depends on the order of the approximation. In general, two equations can be obtained for each pair of sensors located diametrically opposite on the axis:

$$\bar{B}_A = \frac{\hat{B}_{A+} + \hat{B}_{A-}}{2} = \sum_{i=0}^n \left( \sum_{j=0}^n c_{ij} C_{\alpha}^j \right) S_{\beta}^i \quad \text{where } i \text{ is even} \quad (6a)$$

$$\tilde{B}_A = \frac{\hat{B}_{A+} - \hat{B}_{A-}}{2} = \sum_{i=1}^n \left( \sum_{j=0}^n c_{ij} C_{\alpha}^j \right) S_{\beta}^i \quad \text{where } i \text{ is odd} \quad (6b)$$

where  $C$  and  $S$  represent a cosine and a sine function of subscript angles respectively;  $\hat{B}_{A+}$  and  $\hat{B}_{A-}$  denotes that the magnetic flux density measured by the sensors located on the positive and negative side of the ( $A = X$  or  $Y$ ) axis respectively.

Two independent sets of inverse solutions,  $[\hat{\alpha}_1 \ \hat{\beta}_1]$  and  $[\hat{\alpha}_2 \ \hat{\beta}_2]$ , can be solved from the pair of equations; one from each sensor pair. The orientation angles can be estimated as follows:

**Table 1**  
Simulation parameters.

PM	DMP parameters
$ \mathbf{M}  = M\mathbf{e}_z$ , $M = 1.32$ T, diameter = 3.2, length = 12.7 (mm)	$(k = 1, n = 6)$ ; $\bar{e}/\ell = 0.535$ $m_0 = -0.229$ ; $m_1 = 0.618$ Model error = 1%
Sensor/PM location/orientation	$X_s = 0.85$ in., $Z_s = L = 2.75$ in.
Measured magnetic flux	$S_{X\pm} = \pm B_x \mathbf{e}_x$ ; $S_{Y\pm} = \pm B_y \mathbf{e}_y$

$$\begin{bmatrix} \hat{\alpha} \\ \hat{\beta} \end{bmatrix} = \mathbf{W}_1 \begin{bmatrix} \hat{\alpha}_1 \\ \hat{\beta}_1 \end{bmatrix} + \mathbf{W}_2 \begin{bmatrix} \hat{\alpha}_2 \\ \hat{\beta}_2 \end{bmatrix} \quad (7)$$

where  $\mathbf{W}_1$  and  $\mathbf{W}_2$  are the  $2 \times 2$  weighting matrices. For the sensor pair defined in (3ab), the following matrices are chosen due to the symmetry of the sensor-pairs:

$$\mathbf{W}_1 = \begin{bmatrix} 1 & 0 \\ 0 & 0 \end{bmatrix}, \quad \text{and} \quad \mathbf{W}_2 = \begin{bmatrix} 0 & 0 \\ 0 & 1 \end{bmatrix} \quad (8)$$

which indicate the sensor-pairs at  $S_{X\pm}$  and  $S_{Y\pm}$  measure  $\alpha$  and  $\beta$  independently.

### 2.3. Illustrative example

As an illustration, consider a special case using the first order approximation ( $n = 1$ ) for the sensor setup in Fig. 2. With straight-forward substitutions of  $(\hat{B}_{X+}$  and  $\hat{B}_{X-})$  from (4a) into (6a), (6b), and (9) can be obtained from the sensor pair located at  $S_{X\pm}$ ,

$$\begin{bmatrix} \bar{B}_X \\ \hat{B}_X \end{bmatrix} = \begin{bmatrix} (\hat{B}_{X+} + \hat{B}_{X-})/2 \\ (\hat{B}_{X+} - \hat{B}_{X-})/2 \end{bmatrix} = \begin{bmatrix} c_{00} + c_{01} \cos \alpha \\ (c_{10} + c_{11} \cos \alpha) \sin \beta \end{bmatrix} \quad (9)$$

Eq. (9) can be solved to obtain the first estimate  $[\hat{\alpha}_1 \ \hat{\beta}_1]$ :

$$\hat{\alpha}_1 = \cos^{-1} \left( \frac{\bar{B}_X - c_{00}}{c_{01}} \right) \quad \text{and} \quad \hat{\beta}_1 = \sin^{-1} \left( \frac{\hat{B}_X}{c_{10} + c_{11} \cos \hat{\alpha}_1} \right) \quad (10)$$

Similarly, by substituting  $(\hat{B}_{Y+}$  and  $\hat{B}_{Y-})$  from Eqs. (4b) into (6a) and (6b), we have (11) which can be solved for the second estimate  $[\hat{\alpha}_2 \ \hat{\beta}_2]$  in (12):

$$\begin{bmatrix} \bar{B}_Y \\ \hat{B}_Y \end{bmatrix} = \begin{bmatrix} (\hat{B}_{Y+} + \hat{B}_{Y-})/2 \\ (\hat{B}_{Y+} - \hat{B}_{Y-})/2 \end{bmatrix} = \begin{bmatrix} c_{00} + c_{01} \cos \beta \\ (c_{10} + c_{11} \cos \beta) \sin \alpha \end{bmatrix} \quad (11)$$

$$\hat{\alpha}_2 = \sin^{-1} \left( \frac{\hat{B}_Y}{c_{10} + c_{11} \cos \hat{\beta}_2} \right) \quad \text{and} \quad \hat{\beta}_2 = \cos^{-1} \left( \frac{\bar{B}_Y - c_{00}}{c_{01}} \right) \quad (12)$$

Using (10) and (12), the orientation angles can be estimated from (7). Higher-order approximations, though lengthy, can be solved similarly. In general, the inverse solutions become complex as the order  $n$  increases.

### 3. Simulation

To provide insights into the sensing method, we simulate the angular measurement and the magnetic flux density measured by the two sensor-pairs in (3ab) with  $\mathbf{M} = M_0 \mathbf{z}$ . We also compare the absolute orientation among three different orders of approximation in (4a, b). The values of the system parameters used in the simulation are listed in Table 1. The locations of the sensor and the PM for measurement have been chosen to minimize the ef-

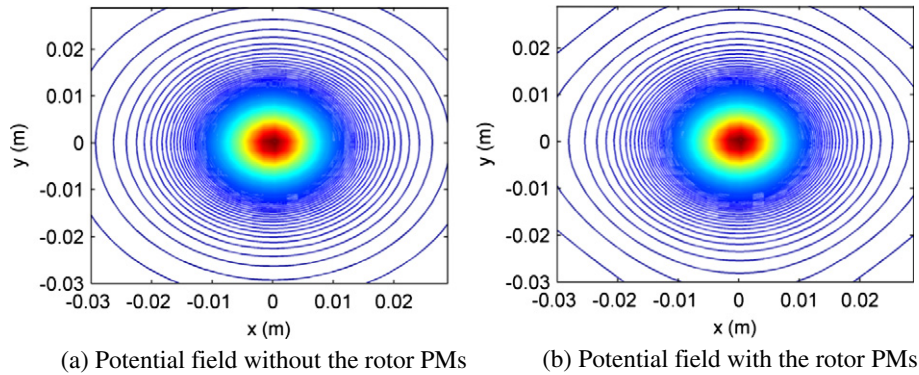


Fig. 3. Potential field at  $(\alpha = \beta = 0)$ .

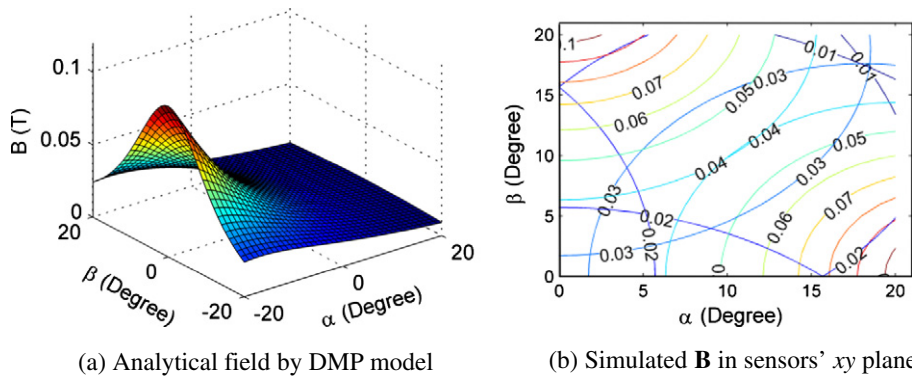


Fig. 4. Simulated measurements.

**Table 2**  
Coefficients for approximation.

Order	Approximation, $c_{ij}$	Max. error (%)
1st	$\begin{bmatrix} -0.319 & 0.344 \\ 1.520 & -1.610 \end{bmatrix}$	17.6
2nd	$\begin{bmatrix} 0.244 & -0.616 & 0.398 \\ -24.63 & 52.137 & -27.622 \\ 92.940 & -195.396 & 102.701 \end{bmatrix}$	8.3
3rd	$\begin{bmatrix} 13.073 & -40.256 & 41.217 & -14.007 \\ -39.768 & 117.58 & -114.792 & 36.89 \\ -1733.83 & 5449.07 & -5709.5 & 1994.51 \\ 5812.28 & -18211.4 & 19019.7 & -6621.01 \end{bmatrix}$	0.9

fects of rotor poles (16 PMs later shown in Fig. 8 and detailed in Table 3) on the sensor sensitivity which of Hall-effect sensor is on average less than one Gauss. Fig. 3 shows potential field and magnetic field  $\mathbf{B}$  with and without the interaction of rotor PMs on the sensor measurement with  $L = 2.75$  in. respectively. Within the range of motion, the rotor PMs does not interfere with the field of the sensing PM.

Given the DMP parameters for the magnetic field and sensor location, Fig. 4a graphs the predicted magnetic flux density  $B_Y$  at  $\mathbf{P}(0, X_S, Z_S)$  over the range of  $\pm 20^\circ$  in  $\alpha$  and  $\beta$  rotations. Since the

sensors are placed symmetrically in the fixed inertial frame, only one sensing quadrant along the positive Y-axis is presented. Based on the analytical DMP models, the coefficients of the 1st, 2nd and 3rd order approximations in (4a,b) are computed using Matlab Optimization toolbox based on the least-square method minimizing the error in (5) and given in Table 2 where 130 samples are used in the range  $-20 \leq \alpha, \beta \leq 20$  ( $^\circ$ ). The simulated errors of the magnetic fields and orientation angles including their Sensitivity are compared in Figs. 5–7 respectively.

As compared in Fig. 5, which plots the magnetic flux densities and their errors, the contours are circular in nature and the sensor readings decrease as the PM moves towards the center; and the maximum error reduces as the approximation order increases. The 3rd order approximation approaches the exact analytical solution with the maximum error within 1%, and its error is relatively uniform over the measured range as compared to the 1st order approximation in  $\alpha$  and  $\beta$  motions.

Sensitivity of the magnetic sensor is investigated to provide the effect of the field measurement and its approximation on performance and accuracy of the measurement. In addition, the analysis can be utilized to determine the weighting matrix  $\mathbf{W}$  in (8). As shown in (13), the sensitivity can be expressed in Jacobian

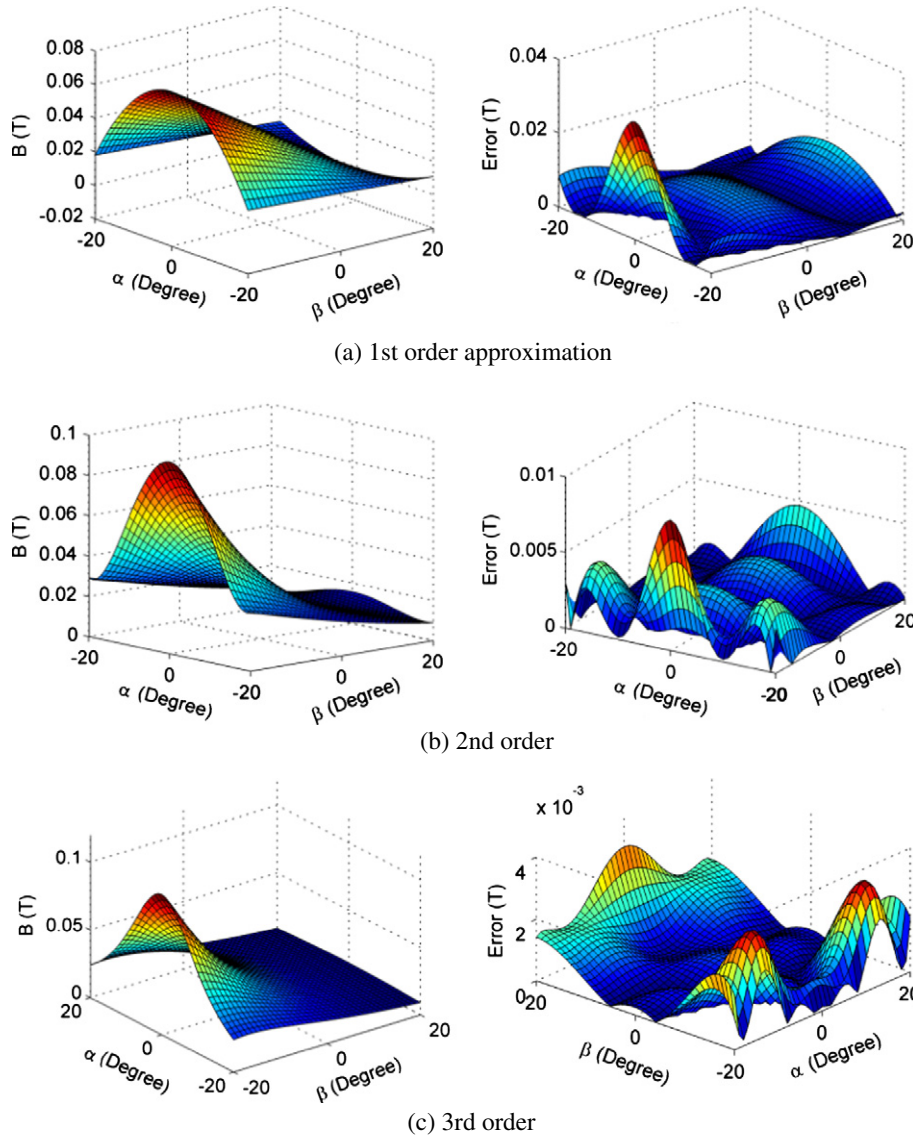


Fig. 5. Approximated magnetic field density.

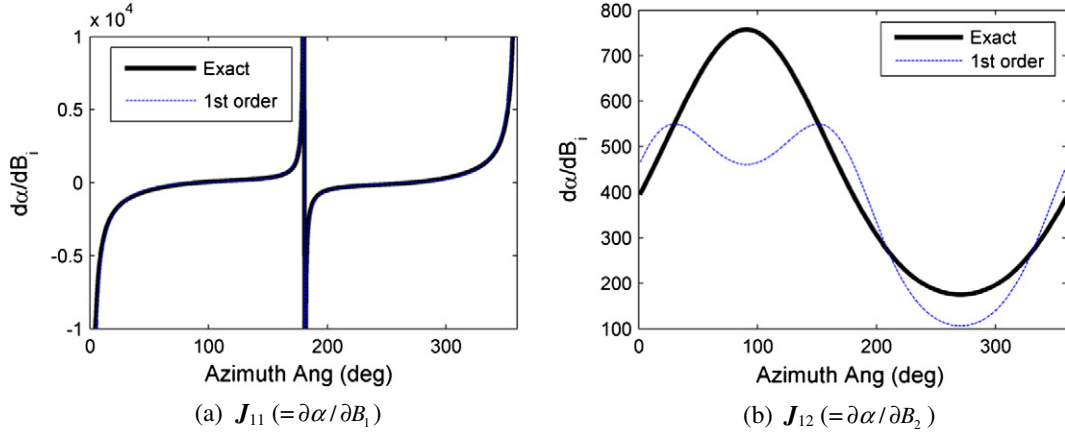


Fig. 6. Sensitivity analysis of the sensor.

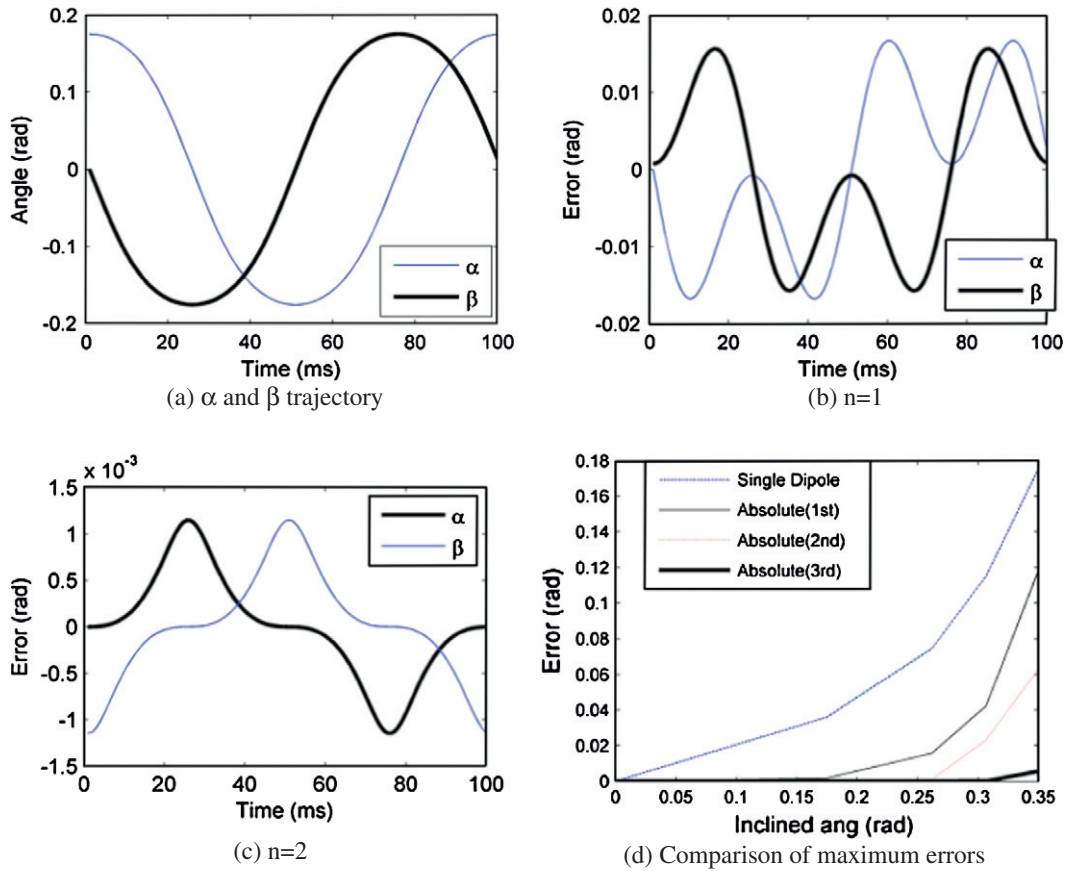


Fig. 7. Simulation of measurement error (at 10° inclination).

matrix with the ratio between measured angle variations and magnetic fields. Thus, larger element in Jacobian indicates less resolution due to larger angle for the given magnetic field variation. Fig. 6 compares the sensitivity of the sensor  $S_{Y+}$  between the DMP model and the 1st order approximation of the model in Fig. 5a when the magnet is moving around a circle ( $-10 \leq \alpha, \beta \leq 10$ ) in the XY plane. It shows the magnetic field variation along the x and y axes with respect to the angle  $\alpha$  respectively. The results indicate that the sensor at  $S_{Y+}$  is better to utilize the magnetic field  $B_{Y\pm}$  or  $\bar{B}_Y$  along the y-axis respect to  $\alpha$ . In other words, the variation of  $\beta$  measured by the sensor  $S_{Y+}$  is less accurate.

$$[\partial\alpha \ \partial\beta]^T = [J][\partial B_k] \quad (13)$$

where  $[J]$  is jacobian matrix of sensitivity defined as  $[J] = \begin{bmatrix} \partial\alpha/\partial B_1 & \dots & \partial\alpha/\partial B_{k_s} \\ \partial\beta/\partial B_1 & \dots & \partial\beta/\partial B_{k_s} \end{bmatrix}$ ; and  $k_s$  denotes the  $k_s^{th}$  sensor (in Fig. 2a).

Fig. 7 analyzes the effect of the polynomial order on the measurement errors (in radians) by comparing different approximation orders for the circular trajectory shown in Fig. 7a where the shaft is inclined at 10° from the Z-axis. As shown in Fig. 7b and c, the measurement errors decrease as the order increases. For the range of

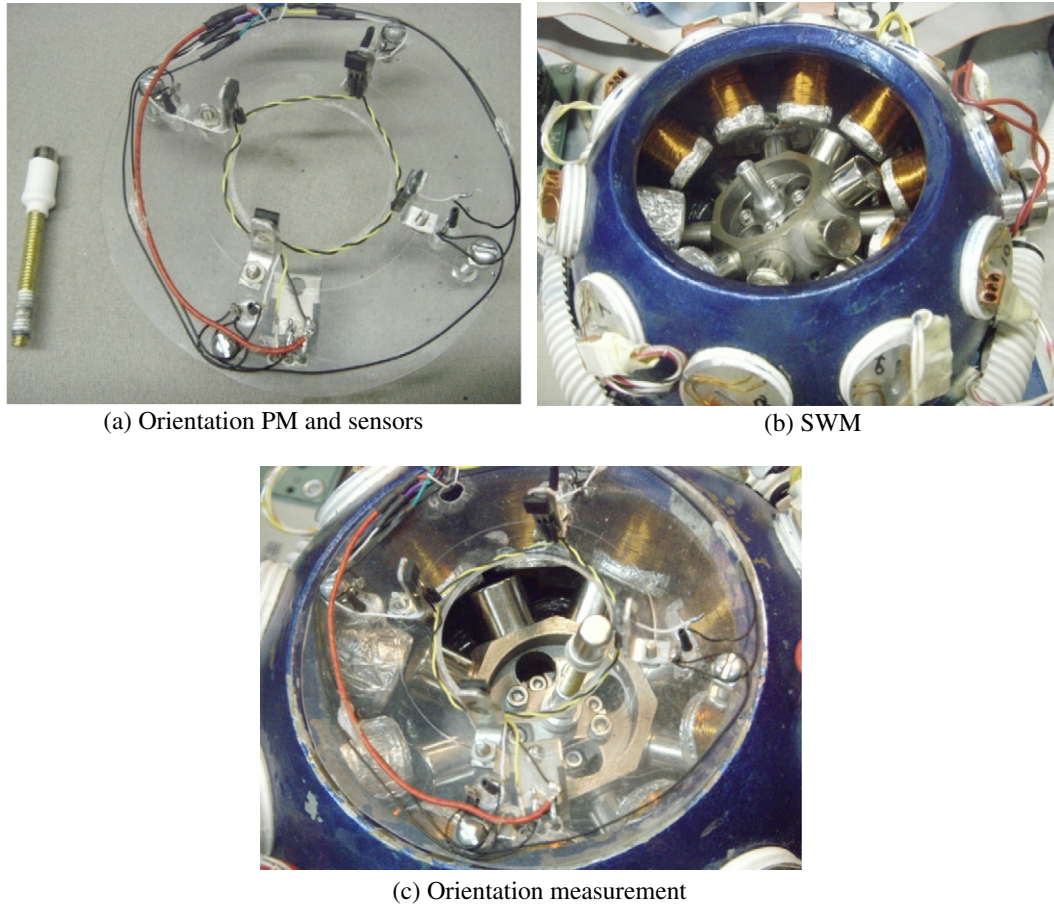


Fig. 8. Spherical wheel motor [15,17] and sensor.

**Table 3**  
Parameters of the SWM.

Rotor	2 Layers of 8 PMs ( $\delta_r = 45^\circ$ )
Radius	76.2 mm (3 in.)
Cylindrical PM	OD = $L = 12.5$ mm (0.5 in.)
Magnetization	$\phi_r^* = 20^\circ$ ; $\delta_r = 45^\circ$ (in.); $\mu_o M_o = 1.35$ T
Stator	2 layers of 10 Ems ( $\delta_s = 36^\circ$ )
Cylindrical EM	OD = 18.8 mm (0.75 in.), 1050 turns, 6.46 $\Omega$
Magnetization	$\phi_s = 26^\circ$ (angle from the horizontal plane); $\delta_s = 36^\circ$ ; AWG 29 coil wire
Air-gap between EM & PM	0.762 mm (0.03 in.)
Moment of rotor inertia (kg m <sup>2</sup> )	$I_o$ (Axial) = 6.0576e-005; $I_t$ (Transverse) = 3.8628e-005

$\phi_r^*$  or  $\phi_s$  indicates an inclination angle from the horizontal plane of the rotor and the stator respectively.

$\pm 20^\circ$  (0.349 radian), errors less than 5  $\mu$  radians can be obtained with the 3rd order approximation while the general single dipole approximation, which neglects the physical dimension of the magnet, offers limited accuracy (Fig. 7d).

#### 4. Experimental results

Fig. 8 shows the spherical wheel motor including four Hall-effect sensors on the top. The Hall-effect sensor (UGN3505) that can measure a wide range of positive and negative magnetic fields is chosen for this experiment. The absolute sensing method is directly applied to measure the orientation of the SWM. Since the magnetization of a permanent magnet installed on the top is

**Table 4**  
Parameters of measurement system.

PM dimension (mm) diameter, length	$B_r$ (T)	$\bar{l}$ (mm)	Coefficients $c_{ij}$ of $\hat{B}$ 1st order	
3.2, 12.7	1.32	6.8	$\begin{bmatrix} -0.0233 & 0.0249 \\ 0.0905 & -0.0945 \end{bmatrix}$	
Sensor parameters				
System I/O	# channels	Range (V)	Update time	Data bit
PCI-DAS6036	16	-10 ~ 10	5 $\mu$ s	16
Sensor	# axis	$V_{cc}$ (V)	$V_{out}$ (V)	Sensitivity
UGN3505	1	5	0.2 ~ 4.7	2.5 mV/G

parallel to the rotor shaft, only orientation of the rotor can be measured.

The output voltage of the sensor is proportional to the strength of the magnetic field with 2.5 mV/Gauss sensitivity under 5 V power supply. The measurement systems are implemented on a personal computer (PC) which has 16 channels of A/D converter (PCI-DAS6036) connected through a signal amplifier. The detail parameters of the SWM and the experimental setup are summarized in Tables 3 and 4.

Prior to the implementation of the Hall-effect sensor on the SWM, the sensor was calibrated using the experimental setup shown in Fig. 9, where the PM and the Hall-effect sensor were separately mounted on two cantilever beams, one of which is driven by a precision NSK ball-screw.

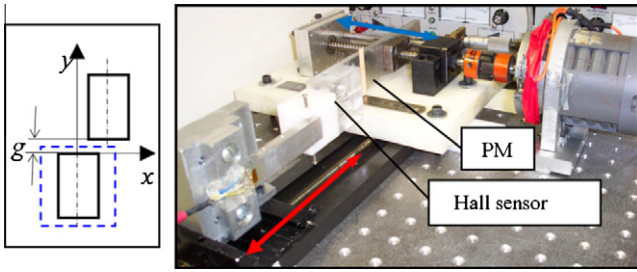


Fig. 9. Experiments on sensor calibration.

The conversion constant  $k_c$  that relates the sensor output voltage to the magnetic flux density was determined by minimizing the error over  $N_s$  samples in (14):

$$E_B = \sum_{i=1}^{N_s} (B - k_{cS_i})^2 \quad (14)$$

where  $B$  is the computed field by the DMP model, and  $S_i$  is the sensor output voltage. The conversion factor  $k_c$  was experimentally determined to be  $k_c = 0.148$ . Fig. 10 compares the experiment and the simulation result of the magnetic flux density  $B$  modeled using the DMP method. Fig. 10a and b compare the  $B_z$  component along the z-axis and the y-axis respectively. When the sensor is closely located at the PM, the voltage output is constant due to sensor saturation, which is shown from 0 (contact) to 5.08 mm (or 0.2 in.) distance in Fig. 10a. The z position at  $z = 12.51$  mm (or 0.65 in.) in Fig. 10b is specified to be the position where the maximum error of the measured  $B_z$  occurred in Fig. 10a. The maximum difference between the measured  $B_z$  and the DMP model is less than 5% for both the y- and z-axes.

Once the sensor calibrated, the permanent magnet was mounted on a tapped shaft of the rotor. The height  $L$  of the magnet can be properly adjusted by the screw rod as shown in Fig. 8. Then, the rotor orientation was measured using the absolute orientation method discussed previously. Two sensor-pairs in the stator frame (Fig. 8) face each other on the X and the Y-axis and measure magnetic flux densities normal to Hall-effect sensors respectively. The values of the PM parameters and flux density approximation in (4a) and (4b) are detailed in Table 4.

Fig. 11a and b compares the experimental and the simulation result obtained for a circular motion using the 1st order approximation in (10) and (12) due to the limited sensor resolution and noise. The circular hole on the sensor base (transparent acrylic plate) shown in Fig. 8 is used as a reference trajectory (XY plane) to measure the orientation. To validate the sensor performance accurately, the experiment is repeated at three times along the same circle contour with the 0.01 s sampling rate. Fig. 11c and d compares the errors obtained experimentally against simulation prediction. Given the sensor performance, their trends agree well and validate that the errors can be analytically predicted by simulation using the DMP method. In addition, the maximum error occurred at every  $45n$  ( $n = 1-4$ ), where the sensor signals are weak. The maximum mean of the errors is 0.012 rad which is an error of less than 10% of the desired inclination.

### 5. Conclusion

This paper presented a novel but simple approach to measure the orientation of a PM-based device in real-time. The method exploits the DMP method to accurately predict magnetic fields unlike conventional magnetic single dipole method that is only valid for a

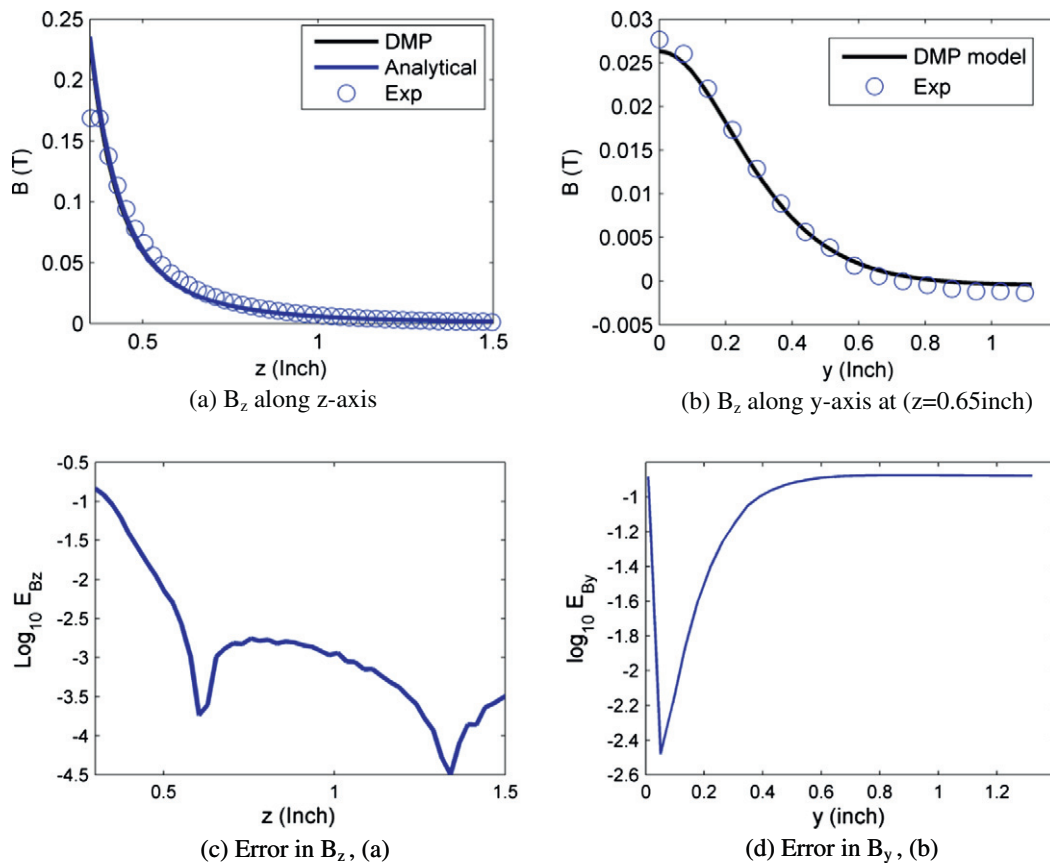


Fig. 10. Hall-effect sensor calibration.

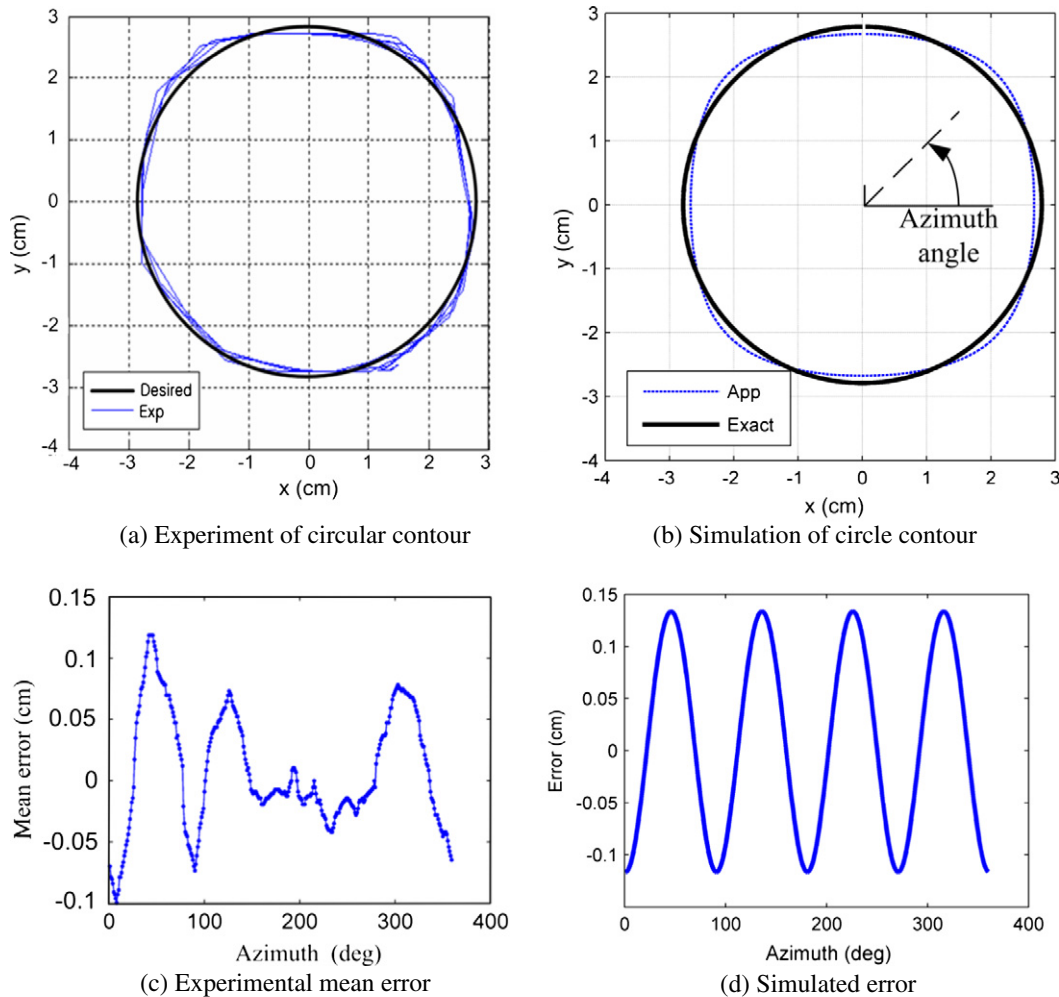


Fig. 11. First order absolute measurement.

needle-shaped PM and utilizes magnetic sensor-pairs to measure the existing magnetic fields such that the rotor orientation is solved inversely from the approximated magnetic field of the DMP method. The ability to characterize the magnetic field in real-time can offer a number of advantages in control, which include: (1) mechanically contact free (eliminating mechanical friction and backlash), compact design since the size of a Hall-effect sensor is relatively small and less mechanical structures (such as linkages) are needed, (2) low-cost efficiency since Hall-effect sensors are generally inexpensive, and (3) relatively high accuracy in real-time computation since the magnetic field can be uniquely predicted by the DMP model.

We illustrated the method by implementing on the SWM to demonstrate its feasibility as a real-time two-DOF orientation sensor. The results comparing the DMP models to the experimental data offer valuable insights to the performance of the methods. Although the performance of the method is not as accurate as existing ones, the method and sensor are still attractive mainly due to contact-free. In addition, it shows feasibility to apply for many engineering applications. The method can be utilized to design a feedback control system for the SWM. Beyond the application of the SWM, it is expected that the method has a potential for a diverse range of PM-based measurements.

#### Acknowledgements

This work is supported in part by SUG Grant from Nanyang Technological University, by Tier 1 Grant from MOE, Singapore,

by the U.S Poultry and Eggs Association and by the Georgia Agricultural Technology Research Program.

#### References

- [1] Paperno E, Sasada I, Leonovich E. A new method for magnetic position and orientation tracking. *IEEE Trans Magn* 2001;37:1938–40.
- [2] Paperno E, Keisar P. Three-dimensional magnetic tracking of biaxial sensors. *IEEE Trans Magn* 2004;40:1530–6.
- [3] Jeong S-H, Rhyu S-H, Kwon BI, Kim B-T. Design of the rotary magnetic position sensor with the sinusoidally magnetized permanent magnet. *IEEE Trans Magn* 2007;43:1837–40.
- [4] Rhyu S-H, Jung O-S, Kwon BI. 2-D modeling and characteristic analysis of a magnetic position sensor. *IEEE Trans Magn* 2005;41:1828–31.
- [5] Lee DV, Velinsky SA. Analysis and experimental verification of a three-dimensional noncontacting angular motion sensor. *IEEE/ASME Trans Mech* 2007;21:612–22.
- [6] Hu C, Meng M-H, Mandal M. A linear algorithm for tracing magnet position and orientation by using three-axis magnetic sensors. *IEEE Trans Magn* 2007;43:4096–101.
- [7] Nara T, Suzuki S, Ando S. A closed-form formula for magnetic dipole localization by measurement of its magnetic field and spatial gradients. *IEEE Trans Magn* 2006;42:3291–3.
- [8] Yabukami S, Kikuchi H, Yamaguchi M, Arai KI, Takahashi K, Itagaki A, et al. Motion capture system of magnetic markers using three-axial magnetic field sensor. *IEEE Trans Magn* 2000;36(5):3646–8.
- [9] Wang J, Jewell G, Howe D. Design and control of a novel spherical permanent magnet actuator with three degrees of freedom. *IEEE/ASME Trans Mech* 2003;8:458–68.
- [10] Jin HZ, Lu H, Cho SK, Lee JM. Nonlinear compensation of a new noncontact joystick using the universal joint mechanism. *IEEE/ASME Trans Mech* 2007;12:549–56.

- [11] Ackermann B, Steinbusch H, Vollmer T, Wang J, Jewell GW, Howe D. A spherical permanent magnet actuator for a high-fidelity force-feedback joystick. *Mechatronics* 2004;14:327–39.
- [12] Sherman JT, Lubkert JK, Popovic RS, DiSilvestro MR. Characterization of a novel magnetic tracking system. *IEEE Trans Magn* 2007;43:2725–7.
- [13] Paperno E, Keisar P. Three-dimensional magnetic tracking of biaxial sensors. *IEEE Trans Magn* 2004;40(3):1530–6.
- [14] Lee K-M, Son H. Distributed multi-pole model for design of permanent-magnet based actuators. *IEEE Trans Magn* 2007;43:3904–13.
- [15] Son H, Lee K-M. Distributed multipole models for design and control of PM actuators and sensors. *IEEE/ASME Trans Mech* 2008;13:228–38.
- [16] Lee K-M, Son H. Design of a magnetic field-based multi degree-of-freedom orientation sensor using the distributed-multiple-pole model. 2007 ASME international mechanical engineering congress and exposition, IMECE2007-42106; November 2007. p. 883–8.
- [17] Son H, Lee K-M. Open-loop controller design and dynamic characteristics of a spherical wheel motor. *IEEE Trans Ind Electron* 2010;57:3475–82.